# ChemComm

Accepted Manuscript


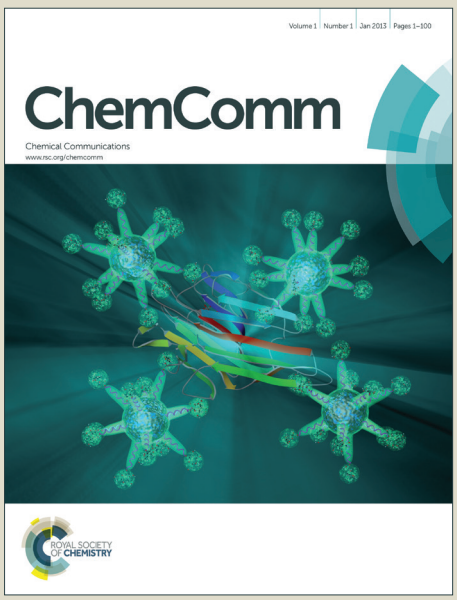





ROYAL SOCIETY OF CHEMISTRY

www.rsc.org/chemcomm

Journal Name

COMMUNICATION

# Single-Molecule Interfacial Electron Transfer Dynamics of Porphyrin on $TiO_2$ Nanoparticles: Dissecting Interfacial Electric Field and Electron Accepting State Density Dependent Dynamics

Received 00th January 20xx,
Accepted 00th January 20xx

DOI: 10.1039/x0xx00000x

www.rsc.org/

Vishal Govind Rao, Bharat Dhital, H. Peter Lu*

**Single-molecule photonstamping spectroscopy correlated with electrochemistry was used to dissect complex interfacial electron transfer (ET) dynamics by probing *m*-ZnTCPP molecule anchored to $TiO_2$ NP surface while electrochemically controlling the energetically-accesible surface states of $TiO_2$ NPs. Application of negative potential raises the electron density in $TiO_2$ NPs, resulting in hinderred forward ET and enhanced backward ET due to the changes of the interfacial electric field and the occupancy of acceptor states. However, density of states plays a dominant role in dictating the interfacial ET dynamics.**

Interfacial electron transfer (ET) mechanism and dynamics at the nanoscale play a critical role in surface chemistry, catalysis, and solar energy conversion, involving significant spatial and temporal complexity and inhomegeneity.[1-10] Hence understanding the underlying rate processes and mechanisms that govern the interfacial ET is imperative. Structure-function studies of different dye-semiconductor systems show that the efficiency of electron injection is guided by the effective electronic and vibronic coupling between dye molecule and semiconductor as well as the free energy driving force associated with the energetic positions of both excited dye molecule and semiconductor conduction band.[8-16] Therefore, tuning relative energetics of the dye excited state relative to the $TiO_2$ accepting states can provide an appropriate control over interfacial ET dynamics, revealing the mechanistic details of the interfacial charge transfer rate process.[11-16] For a system consisting of dye molecules adsorbed on semiconductor nanoparticle (NP) surface, the driving force can be altered by changing the semiconductor Fermi level through an application of potential across semiconductor surface while keeping the energetics of the dye molecule surface binding state constant.[11-15] Studying the interfacial ET dynamics of one molecule at a time in a specific nanoscale local environment, can be highly informative about the underlying processes. For such investigations, single-molecule spectroscopy is particularly powerful in resolving spatiotemporal heterogeneity.[2,17-20] Although single-molecule spectroscopy has ushered in a new era of experimental methodology, it remains challenging to correlate the observed intermittency of interfacial ET dynamics to the fundamental physical properties, such as the driving force, surface state density, and electronic coupling, based on single-molecule fluorescence spectroscopic measurements alone.[21-24]

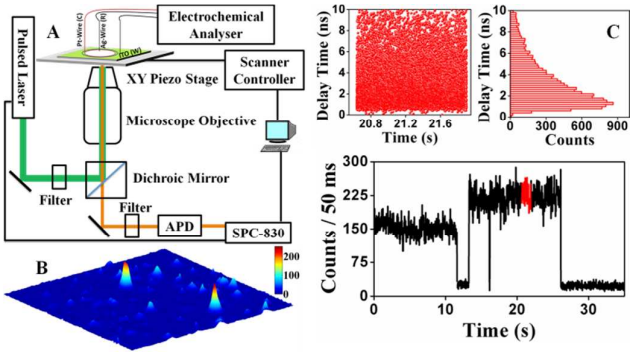


**Fig. 1** (A) Schematic representation of experimental setup for spectroelectrochemistry correlated with photon-stamping spectroscopy. (B) Single-molecule confocal fluorescence images of *m*-ZnTCPP on $TiO_2$ NPs-coated ITO surface with -0.60 V applied potential (10 µm x 10 µm). (C) Typical experimental photon-stamping trajectories for a particular time window (in red) of single-molecule fluorescence intensity trajectory.

Here we report a correlated single-molecule spectroelectrochemistry approach (Figure 1)[25-27] to study the effect of applied electric potential to the interfacial ET dynamics of Zn(II)-5,10,15,20-tetra (3-carboxyphenyl) porphyrin (*m*-ZnTCPP) molecule anchored to $TiO_2$ NP surface in aqueous electrolyte solution. We used single-molecule fluorescence microscopic imaging to obtain single-molecule images of *m*-ZnTCPP (Figure 1B). The bright spot of the image is attributed to a molecular fluorescence of a single *m*-ZnTCPP molecule demonstrating the surface stabilization[28-30] of *m*-ZnTCPP surface-bound to $TiO_2$ NPs.

Figure 2A, 2B, and 2C show the typical single-molecule fluorescence intensity trajectories of *m*-ZnTCPP at different applied potential across the dye-$TiO_2$ interface. At any fixed potential, the blinking behaviour of each single molecule is significantly different from

* *Department of Chemistry and Center for Photochemical Sciences, Bowling Green State University, Bowling Green, Ohio 43403*
*E-mail: hplu@bgsu.edu.*
† Electronic Supplementary Information (ESI) available: Experimental detail, AFM data, spectroscopy data. See DOI: 10.1039/x0xx00000x

others. However, for majority of the molecules the blinking pattern is dominated by dark states in case of zero and positive applied potential (Figure 2A and 2C), whereas in case of negative applied potential we observed a quasi-continuous (intensity trajectory with no distinct bright and dark states) distribution of fluorescence intensities (Figure 2B). The observed single-molecule fluorescence time trajectories have the characteristic blinking between bright and dark states in absence of applied potential (Figure 2A), which is associated with temporal fluctuation or dynamic disorder of interfacial ET dynamics.[2,18,20] To explain how the applied potential significantly alters the blinking behavior of the molecules, we need to examine the underlying processes that contribute to blinking. The uniqueness of single-molecule photonstamping spectroscopy lies in the fact that for each photoexcitation, if the excited state of the dye molecule involves an ultrafast forward electron transfer (FET) process reaching a charge-separation state of a oxidized dye and an excess electron in $TiO_2$, then the dye molecule will not emit a photon through an S1 to S0 radiative transition (Figure 3). The oxidized dye is mostly nonfluorescent, and the dye molecule can only emit another photon when a backward electron transfer (BET) occurs reducing the oxidized dye back to a ground state, S0. Therefore, a close look of single-molecule fluorescence intensity trajectories can provide information about FET and BET dynamics. For each photoexcitation, the excited state of the single-molecule either undergoes radiative emission to yield an emission photon that contributes to a bright state or undergoes a nonradiative interfacial ET process that contributes to the dark state. The occurrence of the dark and bright states is ultimately determined by the dominance of radiative or the nonradiative interfacial ET rate process, which further depends on the other ET rate regulating parameters, such as the electronic and vibrational coupling between the molecule and the substrate.[2,8-16,18,20,31,32] Following an interfacial ET to $TiO_2$, the injected electrons go through charge trapping, detrapping, and electron Brownian and non-Brownian diffusion before mostly recombining with parent oxidized dye, the BET.[2,8,11,13,15] Surface traps play an important role in dynamics of injected electrons in $TiO_2$. Therefore, a fundamental understanding of the surface states, such as their nanoscale distribution and involved charge transfer coupling, is crucial to the improvement of the photoelectrical performance of semiconductor materials.[8,11,13,15,22] Previously, a near-field scanning microscopic imaging analysis of surface states on a $TiO_2$ (110) surface was demonstrated and reported.[22a] We have shown that for a molecule adsorbed on the semiconductor surface, the surface state charge-transfer pathways are primarily affected by the density and energy distributions of the surface states.[22a]

The BET rate depends on the time spent by an excess electron on $TiO_2$ NPs, which further depends on the distribution of excess electron trap states within the NPs. Consequently, the BET rate typically influence the blinking behavior of the single-molecules anchored to $TiO_2$ NPs. The BET process, i.e., the excess electron and oxidized dye recombination, has been reported to occur in the range of picoseconds (ps) to several milliseconds (ms) under various cross interfacial electric bias conditions.[11-14,33,34] Therefore, considering the nanosecond radiative relaxation lifetime of the excited state of *m*-ZnTCPP and the picoseconds to milliseconds timescale of BET, we attribute that fluorescence fluctuation

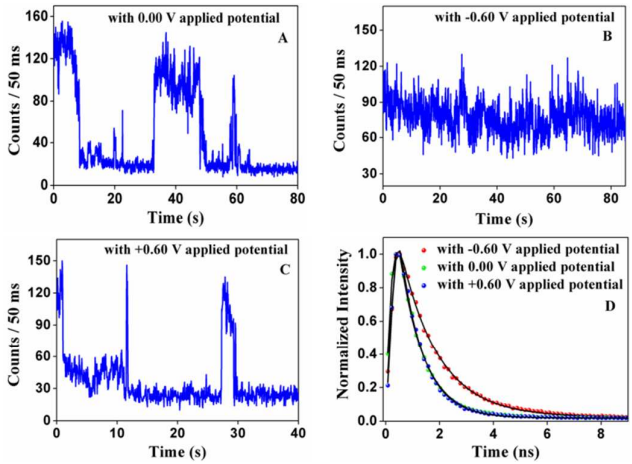


**Fig. 2** Single-molecule fluorescence intensity trajectories of *m*-ZnTCPP on $TiO_2$ NPs-coated ITO surface in presence of 0.1 M NaCl aqueous electrolyte with (A) 0.00 V, (B) -0.60 V, and (C) +0.60 V applied potential. (D) Series of single-molecule fluorescence decays with different applied potentials.

dynamics strongly depends on BET rate. If the BET time is in the order of ms-µs, longer than ns radiative relaxation time of the excited state of a dye molecules, then the dye molecule will be expected to spend more time in a given charge state $M/M^+$ (M = *m*-ZnTCPP). This leads to slow switching between M and $M^+$ within the bin time, resulting in distinct bright and dark states. On the other hand, if the BET time is of the order of ns-ps, faster than the ns radiative relaxation time, then the dye molecule will be expected to spend less time in a given charge state $M/M^+$ leading to fast switching between M and $M^+$ within the bin time, which results in a quasi-continuous distribution of fluorescence intensities.

The preceding discussion attests to the fact that the observed quasi-continuous distribution of fluorescence intensities at applied negative potential (Figure 2B) can be attributed to either (i) absence of FET at applied negative potential or (ii) fast BET rate. Literature reports suggest that the decrease in FET rate with applied negative potential is minimal (5-25 times) compared to the enhancement in BET rate ($10^3$-$10^8$ times).[11-14] For $TiO_2$ NPs the BET rate was found to be in the rage of milliseconds to microseconds at positive or zero applied potential, whereas a dramatic increase in recombination rate (in the rage of nanoseconds to picoseconds) has been reported at negative potential.[11-14] Hence here the substantial increment in BET rate is deemed to be the determining factor for the observed change in blinking pattern. This behavior can be further explained by considering the modulation of Fermi level of $TiO_2$ NP as well as the changed electron occupancy in $TiO_2$ conduction band (CB) and energetically accessible surface traps states under the applied electric bias (Figure 3). Several previous reports have indicated the existence of a high density of sub-bandgap or trap states lying below the CB of $TiO_2$ NPs, which results in an exponential tail to the CB density of states.[2,8,10,12-15,22] With the application of negative potential, the Fermi level approaches or exceeds the potential of CB acceptor states/trap states, which results in occupancy of these states (Figure 3).[8,10,12-15] Higher occupancy of CB acceptor states/trap states as well as increased electron density supports a higher BET rate.[8,12-15,35,36] However, applied positive bias does not

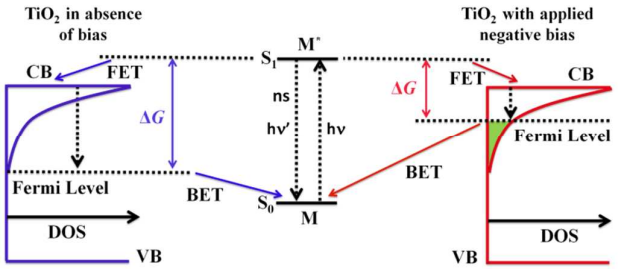


**Fig. 3** Schematic illustration of the effect of applied negative bias on the $TiO_2$ sub-bandgap or trap states. DOS, density of states; and VB, valence band. The applied negative potential raises the $TiO_2$ Fermi level, which leads to occupancy of CB electron acceptor states. Green areas denote electron acceptor states unavailable for ET from *m*-ZnTCPP excited state.

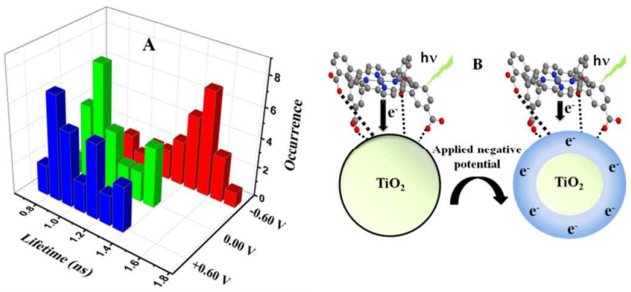


**Fig. 4** Fluorescence lifetime distributions of *m*-ZnTCPP on $TiO_2$ NPs-coated ITO surface in presence of 0.1 M NaCl aqueous electrolyte with +0.60 V, 0.00 V and -0.60 V applied potential. (B) Schematic depiction of interfacial ET in absence and presence of applied electric bias. In absence of electric bias the efficiency of photoinduced ET is high (indicated by large arrow), whereas the application of negative potential raises the electron density in $TiO_2$ NPs, leading to decrease in the efficiency of ET (indicated by small arrow).

affect the density of electron accepting states of $TiO_2$ NPs and has no effect on BET rate and blinking behavior (Figure 2).[12-15] Plausibly, the higher BET rate can be assigned to the observed quasi-continuous distribution of fluorescence intensities of *m*-ZnTCPP. The dependence of BET rate upon applied bias has already been reported and modelled as a random walk between an exponential energetic distribution of trap sites.[37,38] This random walk model was also suggested by our earlier single-molecule interfacial ET dynamics studies with *p*-ZnTCPP and *m*-ZnTCPP along with other literature reports.[18,20,39,40] We have shown power-law distribution of dark times, related to geminate recombination dynamics, dominant by Lévy statistics.[18,20,41] The combination of our findings partially reveals the role of trap sites on interfacial ET dynamics. This, by far, is the first report of an indirect evidence of BET rate at single molecule level.

To further dissect the complex interfacial electron transfer dynamics, we have studied the effect of driving force on FET and hence on the lifetime of *m*-ZnTCPP. The increase in the lifetime of *m*-ZnTCPP molecule anchored to $TiO_2$ NP surface with applied negative potential (Figure 2D) indicates decrease in ET efficiency. Figure 4A shows single-molecule fluorescence lifetime distributions of *m*-ZnTCPP molecules at different applied potential. The lifetime distribution from 0.7 ns to 1.4 ns with 0.00 V applied potential clearly demonstrates the individuality of each molecule in a specific environment associated with the inhomogeneous surface state distribution of *m*-ZnTCPP molecules on rough $TiO_2$ NP surface. The shift towards longer lifetime indicates retardation of FET rate with applied negative potential. This retardation can be assigned to (i) an increase in electron density within the $TiO_2$ CB (Figure 4B), which reduces the density of unoccupied states available for electron injection and (ii) decrease of the FET free energy driving force (Figure 3).[12-15] Nevertheless, compared to eight order of magnitude change of BET rate the FET rate changes only by one order of magnitude.[11-14] The Fermi level of $TiO_2$ with applied negative potential (in our working range) lies within the Schottky barrier, and only states near the band edge are filled (Figure 3).[4c,36] So most electron accepting states of $TiO_2$ CB with applied negative potential remain unoccupied and the density of accepting states for ET from excited *m*-ZnTCPP molecule should not be significantly smaller than *m*-ZnTCPP on $TiO_2$ NPs.

It should be noted that our measurements only consider those molecules which are visible in single-molecule confocal fluorescence images. The visibility of single molecules suggests that the FET time fluctuates in a wide time scale from femtoseconds to nanoseconds or even slower. The lifetime variation range with applied potential also indicates presence of a time component having nanosecond fluctuation of FET. Had the time scale of the FET been solely in the femtosecond to picosecond range, the excited state radiative emission efficiency would have been as low as $10^{-3}$ to $10^{-6}$ and the single molecules would essentially be undetectable by photon detection. This highly inhomogeneous interfacial electron transfer processes are well supported by ensemble-averaged time-resolved data in the literature.[42]

Even though the change in blinking pattern as well as the lifetime distributions of single *m*-ZnTCPP molecules demonstrates the correlation between the applied electric potential across $TiO_2$/ITO electrode and the kinetics of interfacial ET dynamics, it is desirable to investigate perticular single molecules in identical conditions. To illustrate this we monitored fluorescence intensity trajectories and fluorescence lifetime of *m*-ZnTCPP molecules anchored to $TiO_2$ NPs surfaces modulated by cyclic voltammetric (CV) potential scanning (Figure 5). The fluorescence intensity level increases and decreases with ramping down (scanning from +0.6 V to -0.6 V) and ramping up (scanning from -0.6 V to +0.6 V) the voltage, respectively. The higher fluorescence intensity with applied -0.6 V potential than +0.6 V demonstrates less fluorescence quenching due to reduced interfacial electron transfer at -0.6 V potential. The lifetime for the two regions of Figure 5A, marked in red and blue were derived using photon stamping spectroscopy. The lifetime obtained for red region (1.0 ns) is higher than the blue region (0.8 ns), which again reflects decrease in ET efficiency at negative potential. However, the small change in lifetime is well supported by literatures reports showing minimal effect of applied bias on FET rate.[11-14]

In conclusion we can control the blinking behavior of single-molecule anchored to $TiO_2$ NPs with applied electric potential by effectively tuning electron density inside the $TiO_2$ NPs. The applied negative potential causes (i) decrease in charge injection efficiency resulting in higher excited state lifetime of *m*-ZnTCPP and ii) increase in BET rate following charge injection resulting in quasi-continuous intensity variation. However, the applied positive bias has essentially no effect on blinking behavior and lifetime, which

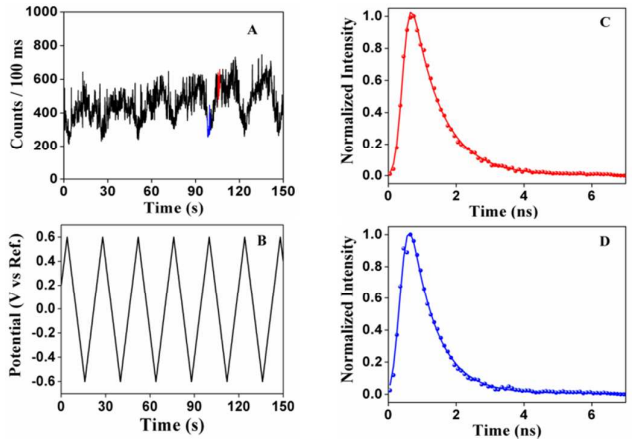


**Fig. 5** Single-molecule spectroelectrochemistry of *m*-ZnTCPP on $TiO_2$ NPs-coated ITO surface in presence of 0.1 M NaCl aqueous electrolyte: (A) single-molecule fluorescence intensity trajectory obtained during the CV scanning. (B) Potential *vs.* time plot of the CV scan. (C), (D) fluorescence decays derived from different time window of the trajectory shown in (A).

indicates that density of states plays a dominant role in dictating the changes in rates of charge transfer in our system. This is further supported by the preliminary results of our ongoing study on the role of density of accepting state in semiconductors that have similar density of states but large difference in driving force. Our single molecule spectroelectrochemical study provides novel insights in determining the nature of semiconductor energy states that participate in interfacial ET.

This work is supported by the Office of Basic Energy Sciences within the Office of Science of the U.S. Department of Energy (DOE).

## Notes and references

1 (a) A. Hagfeldt and M. Grätzel, *Acc. Chem. Res.*, 2000, **33**, 269; (b) S. Mathew, A. Yella, P. Gao, R. Humphry-Baker, B. F. Curchod, N. Ashari-Astani, I. Tavernelli, U. Rothlisberger, M. K. Nazeeruddin and M. Grätzel, *Nature Chem.*, 2014, **6**, 242.
2 (a) V. Biju, M. Micic, D. Hu and H. P. Lu, *J. Am. Chem. Soc.*, 2004, *126*, 9374; (b) L. Guo, Y. Wang and H. P. Lu, *J. Am. Chem. Soc.*, 2010, **132**, 1999.
3 P. G. Johansson, A. Kopecky, E. Galoppini and G. J. Meyer, *J. Am. Chem. Soc.*, 2013, **135**, 8331.
4 (a) K. Zheng, K. Žídek, M. Abdellah, P. Chábera, M. S. Abd El-sadek and T. Pullerits Appl. Phys. Lett., 2013, **102**, 163119; (b) A. A. Cordones and S. R. Leone, *Chem. Soc. Rev.*, 2013, **42**, 3209. (c) S. jin, N. Song and T. Lian, *Acs Nano*, 2010, **4**, 1545.
5 S. Ye, A. Kathiravan, H. Hayashi, Y. Tong, Y. Infahsaeng, P. Chabera, T. r. Pascher, A. P. Yartsev, S. Isoda, H. Imahori and V. Sundström, *J. Phys. Chem. C*, 2013, **117**, 6066.
6 B. Farnum, Z. Morseth, M. K. Brennaman, J. Papanikolas and T. J. Meyer, *J. Am. Chem. Soc.*, 2014. **136**, 15869.
7 (a) P. V. Kamat, *J. Phys. Chem. Lett.*, 2012, **3**, 663; (b) P. V. Kamat, and I. Bedja, *J. Phys. Chem.*1996, **100**, 4900.
8 N. A. Anderson and T. Lian, *Annu. Rev. Phys. Chem.*, 2005, **56**, 491.
9 (a) W. R. Duncan and O. V. Prezhdo, *Annu. Rev. Phys. Chem.*, 2007, **58**, 143; (b) Z. Yao, M. Zhang, R. Li, L. Yang, Y. Qiao and P. Wang, *Angew. Chem. Int. Ed.*, 2015, **54**, 5994.
10 D. F. Watson and G. J. Meyer, *Annu. Rev. Phys. Chem.*, 2005, **56**, 119.
11 S. A. Haque, Y. Tachibana, D. R. Klug and J. R. Durrant, *J. Phys. Chem. B*, 1998, **102**, 1745.
12 S. E. Koops, B. C. O'Regan, P. R. Barnes and J. R. Durrant, *J. Am. Chem. Soc.*, 2009, **131**, 4808.
13 Y. Tachibana, S. A. Haque, I. P. Mercer, J. R. Durrant and D. R. Klug, *J. Phys. Chem. B*, 2000, **104**, 1198.
14 S. A. Haque, Y. Tachibana, R. L. Willis, J. E. Moser, M. Grätzel, D. R. Klug and J. R. Durrant, *J. Phys. Chem. B*, 2000, **104**, 538.
15 (a) I. J. McNeil, L. Alibabaei, D. L. Ashford and C. J. Fecko, *J. Phys. Chem. C*, 2013, **117**, 17412; (b) R. Godin, B. D. Sherman, J. J. Bergkamp, C. A. Chesta, A. L. Moore, T. A. Moore, R. E. Palacios, and G. Cosa, *J. Phys. Chem. Lett.*, 2015, **6**, 2688.
16 R. N. Sampaio, R. M. O'Donnell, T. J. Bar and G. J. Meyer, *J. Phys. Chem. Lett.*, 2014, **5**, 3265.
17 H. P. Lu and X. S. Xie, *Nature*, 1997, **385**, 143.
18 Y. Wang, X. Wang, S. K. Ghosh and H. P. Lu, *J. Am. Chem. Soc.*, 2009, **131**, 1479.
19 V. B. Leite, L. C. Alonso, M. Newton and J. Wang, *Phys. Rev. Lett.*, 2005, **95**, 118301.
20 V. G. Rao, B. Dhital, Y. He and H. P. Lu, *J. Phys. Chem. C*, 2014, **118**, 20209.
21 D. Pan, N. Klymyshyn, D. Hu and H. P. Lu, *Appl. Phys. Lett.*, 2006, **88**, 093121.
22 (a) P. C. Sevinc, X. Wang, Y. Wang, D. Zhang, A. J. Meixner and H. P. Lu, *Nano Lett.*, 2011, **11**, 1490; (b) X. Wang, D. Zhang, Y. Wang, P. Sevinc, H. P. Lu and A. J. Meixner, *Angew. Chem. Int. Ed.*, 2014, **50**, A25.
23 Z. Liu, H. Zhu, N. Song and T. Lian, *Nano Lett.*, 2013, **13**, 5563.
24 D. Zhang, U. Heinemeyer, C. Stanciu, M. Sackrow, K. Braun, L. Hennemann, X. Wang, R. Scholz, F. Schreiber and A. J. Meixner, *Phys. Rev. Lett.*, 2010, **104**, 056601.
25 R. E. Palacios, F.-R. F. Fan, A. J. Bard and P. F. Barbara, *J. Am. Chem. Soc.*, 2006, **128**, 9028.
26 C. Galland, Y. Ghosh, A. Steinbrück, M. Sykora, J. A. Hollingsworth, V. I. Klimov and H. Htoon, *Nature*, 2011, **479**, 203.
27 W. F. Paxton, S. L. Kleinman, A. N. Basuray, J. F. Stoddart and R. P. Van Duyne, *J. Phys. Chem. Lett.*, 2011, **2**, 1145.
28 A. K. Vannucci, L. Alibabaei, M. D. Losego, J. J. Concepcion, B. Kalanyan, G. N. Parsons and T. J. Meyer, J. *Proc. Natl. Acad. Sci. U. S. A.*, 2013, **110**, 20918.
29 D. G. Brown, P. A. Schauer, J. Borau-Garcia, B. R. Fancy and C. P. Berlinguette, *J. Am. Chem. Soc.*, 2013, **135**, 1692.
30 S. Rangan, S. Coh, R. A. Bartynski, K. P. Chitre, E. Galoppini, C. Jaye and D. Fischer, *J. Phys. Chem. C*, 2012, **116**, 23921.
*31* T. Tachikawa, N. Wang, S. Yamashita, S. C. Cui and T. Majima, *Angew. Chem. Int. Ed.*, 2010, **49**, 8593.
32 T. Tachikawa, S. Yamashita and T. Majima, *J. Am. Chem. Soc.*, 2011, **133**, 7197.
*33* D. Liu, R. W. Fessenden, G. L. Hug and P. V. Kamat, *J. Phys. Chem. B*, 1997, **101**, 2583.
34 S. G. Yan and J. T. Hupp, *J. Phys. Chem.*, 1996, **100**, 6867.
35 Y. Bai, I. n. Mora-Seró, F. De Angelis, J. Bisquert and P. Wang, *Chem. Rev.*, 2014, **114**, 10095.
36 E. Palomares, J. N. Clifford, S. A. Haque, T. Lutz and J. R. Durrant, *J. Am. Chem. Soc.*, 2003, **125**, 475.
37 I. Mora-Seró and J. Bisquert, *Nano Lett.*, 2003, **3**, 945.
38 J. Nelson, *Phys. Rev. B*, 1999, **59**, 15374.
39 G. Margolin and E. Barkai, *J. Chem. Phys.*, 2004, **121**, 1566.
40 L. C. Paula, J. Wang and V. B. Leite, *J. Chem. Phys.*, 2008, **129**, 224504.
41 (a) I. J. McNeil, D. L. Ashford, H. Luo, and C. J. Fecko, *J. Phys. Chem. C*, 2012, **116**, 15888; (b) N. Z. Wong, Al. F. Ogata, and K. L. Wustholz, *J. Phys. Chem. C*, 2013, **117**, 21075.
42 Moser, J. E. *Dye-Sensitized Solar Cells*, EPFL Press, Lausanne, Switzerland, 2010, and references therein.